Slow Crack Growth in Single-Crystal Silicon

J. A. Connally and S. B. Brown

Time-dependent crack growth has been measured on a precracked, single-crystal silicon cantilever beam 75 micrometers long that was excited at resonance. Growth of the precrack changes the resonant frequency of the beam, which is correlated to crack length. The measured steady-state crack growth rate was as slow as 2.9×10^{-13} meter per second, although the apparatus can measure crack growth rates as low as 10^{-15} meter per second. It is postulated that static fatigue of the native surface silica layer is the mechanism for crack growth. These experiments demonstrate the possibility of rate-dependent failure of silicon devices and the applicability of linear elastic fracture mechanics to small-scale micromechanical devices. The results indicate that slow crack growth must therefore be considered when evaluating the reliability of thin-film silicon structures.

The increasing use of small micromechanical devices and advanced sensors has led to concern about the failure modes and reliability of these structures. For example, the intended lifetime of micromechanical devices now being fabricated for use in automobiles, aircraft, and satellites can easily exceed 10 years (*1*). Other applications include biomedical instruments where reliability is the primary design criterion. More sophisticated packaging of electronic devices is similarly increasing the complexity of material interconnects, with accompanying uncertainty about the interconnect reliability.

A poorly characterized aspect of the mechanical response of all of these structures is the time-dependent propagation of cracks within the structures. It is not possible to fabricate these structures without defects or stress concentrations. Thermal or mechanical cycling coupled with incompatible mechanical and thermal properties will inevitably give rise to stress states that can cause a crack to nucleate or a preexisting crack to grow. Moreover, some small-scale structures are designed to function within severe environments, where chemical processes can create or accelerate crack growth. These environments do not have to be exotic, for the presence of water can easily produce static fatigue in silica (*2*, *3*) and in silicon.

It is not apparent that failure modes obtained on a macroscopic scale extend to the scale of smaller structures. The mechanisms that govern large-scale failure on standard macroscopic, laboratory specimens may not necessarily be those that govern the failure of smaller structures. At some scale, continuum assumptions will no longer be valid. Surface coatings, microstructural and surface features, and interface thicknesses then become large relative to the structure's dimensions.

Our initial work suggests that static fatigue on the microscopic scale does not duplicate macroscopic static fatigue; fatigue limits and dependence on stress intensity may be different. Our results suggest that water-induced, slow crack growth may occur in silicon devices by static fatigue of the silica layer that forms immediately when silicon is exposed to oxygen.

Previous work on static fatigue of silicon has been inconclusive. Chen and Knapp (*4*) performed stress corrosion experiments with single-crystal silicon bars that were precracked with a Knoop microhardness tester and statically loaded in four-point bending. The surface of the beam was wetted with various liquids including distilled water, and the time to fracture recorded. The loading was on the order of 95% of the static fracture load. The beams were monitored for up to 2 weeks. None failed, and Chen and Knapp concluded that stress corrosion cracking does not occur. Wong and Holbrook (*5*) performed a similar experiment in which single-crystal silicon wafers were indented and cracked with a microhardness tester. The radial crack lengths were measured as a function of time in both ambient air and deionized water. No crack growth was observed, so they concluded that stress corrosion cracking does not occur because of the formation of a protective silica layer. Bhaduri and Wang (*6*) observed a crack growth process in larger scale, double-torsion silicon specimens using load relaxation. However, other investigators were not able to duplicate their results. Chen and Leipold (*7*) subsequently performed similar double-torsion experiments and concluded that slow crack growth does not occur in silicon. Thouless and Cook (*8*) demonstrated that indented silicon would spall if placed in HF acid, but they were unable to find any effect due to water and were not able to measure crack growth rates given the simplicity of their experiments. The results obtained with our fatigue specimen are unambiguous; crack growth occurs at a very small but measurable rate.

A limited amount of fracture testing has been performed with small-scale silicon structures. Excepting our work, to our knowledge no research has been done with respect to time-dependent failure. Several investigators have used cantilever beams to examine mechanical properties. Weihs *et al.* (*9*) and Johansson *et al.* (*10*) examined yield stresses, elastic properties, and breaking strength using micromechanical cantilever beams. Their failure measurements were approximate, however, because the concentration of stress was dependent on the particular geometry of the beam; they did not introduce a crack. Fan *et al.* (*11*) presented some micromechanical bridge geometries involving stress concentrations. These geometries were not statically determinant, nor were cracks introduced into the bridges. Residual stresses were introduced during fabrication, so the state of stress was not precisely known. Fan and his collaborators also did not consider rate-dependent behavior because failure of their structures occurred in the last stage of fabrication.

We have investigated rate-dependent crack growth in a small specimen of silicon that is sensitive to small changes in crack length. A cantilever beam is formed by diffusing boron into a silicon wafer and then etching around the structure with an anisotropic etch (Fig. 1). At the free end of the cantilever is a rectangular plate 150 μm wide and 235 μm long, which provides area for electrostatic forcing and sensing, and gold plating that serves as a counterweight to lower and adjust the resonant frequency. The volume etched beneath the beam and plate extends to a depth of ~130 μm. Gold bridge electrodes extending across the specimen electrostatically drive the cantilever and sense its motion. We use a nanoindenter to introduce a linear array of surface indentations that link to create a precrack approximately 2 to 3 μm deep across the thickness of the beam, 10 μm from the

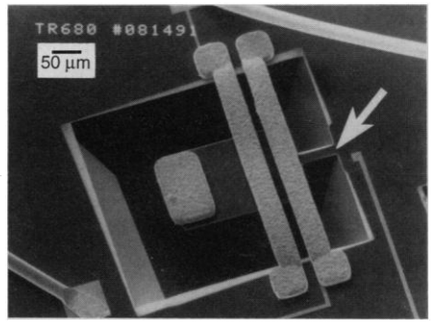

Fig. 1. Scanning electron micrograph of a micromechanical specimen of silicon. Gold electrodes extend over the specimen. A crack is introduced at the site indicated by the arrow, 10 μm from the base of the beam.

Department of Materials Science and Engineering, Massachusetts Institute of Technology, Cambridge, MA 02139.

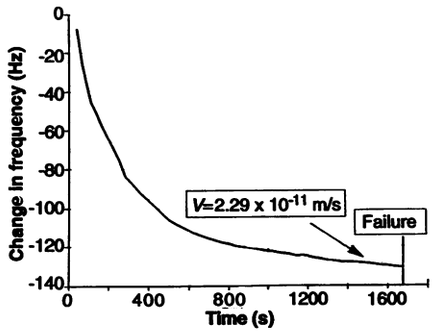

Fig. 2. Change in frequency versus time indicating increasing crack length. The specimen failed at the point indicated. The final crack growth rate V was estimated to be approximately 2.3×10^{-11} m/s.

base. A control system excites the device at resonance, generating large displacements that create a high axial stress component at the base of the beam.

An extension of this crack reduces the total stiffness of the beam, causing a significant change in resonant frequency, by which crack growth is detected. Every increase in crack length of 2.5 nm corresponds to approximately a 1-Hz change in resonant frequency. We use a dynamic model to correlate both the resonant frequency to crack length and the amplitude of motion to stress intensity. The model is a lumped system model with three degrees of freedom and includes the change in compliance due to the deep cracked beam (*12*), the effect of crack closing and opening, and the effects of viscous damping around the specimen (*13*). The dynamic model has been calibrated to measurements of frequency and compliance of both cracked and uncracked devices. We have also constructed a finite-element model of the uncracked device and obtained excellent correlation between the finite-element modal frequencies and the resonant frequency predicted by the dynamic model (*13*).

The method of fatigue testing proposed in this experiment is analogous to compliance testing on a macro scale where a constant load or displacement is applied to a precracked specimen and the corresponding change in load or displacement is measured as a function of time and correlated to crack growth (*14*). In this experiment, the frequency corresponds to a specific crack length. A change in frequency corresponds to a stiffness change at the crack site, which in turn corresponds to a change in crack length.

We maintain the device at resonance using a phase control system that holds the response of the device at a 90° phase angle from the excitation. A linear first-order transfer function models any phase deviations and is valid for small perturbations near the resonant frequency. A frequency counter then measures the frequency as a function of time. The first bending mode of the cantilever and end plate system has a frequency of approximately 12,000 Hz. The finite-element analysis indicates that the second and third modes are combinations of torsion about the lengthwise axis of the beam and out-of-plane bending. Although the dynamic analysis using the model was two-dimensional, the out-of-plane coupling is a negligibly small static response.

The accuracy and stability of frequency measurements give us the capability of measuring crack growth increments on the order of nanometers over a period of weeks, which translates to an averaged crack growth rate as slow as 10^{-15} m/s. The range of measurable crack growth rates therefore spans the range of rates starting at approximately 10^{-7} m/s to the slowest of 10^{-15} m/s, representing eight orders of magnitude. This lower rate indicates that our technique is significantly more sensitive than double-torsion methods.

Linear elastic fracture toughness measured with this device correlates with published values for single-crystal silicon. Chen and Leipold (*15*) measured fracture toughness using indented, four-point-bend specimens, obtaining a value of 0.82 $N/m^{3/2}$. We tested a precracked fatigue specimen under static loads using a nanoindenter and obtained a fracture toughness of 0.65 $N/m^{3/2}$. The lower value may be due to our assumption of a rectangular cross section for the beam, whereas the actual specimen cross section more closely approximates an ellipse.

Figure 2 is a plot of the change in frequency versus time for an experiment in humidified air in which a precracked device was tested until failure. This experiment is typical in that there is an initially rapid change in frequency rate that subsequently decreases to a very low rate of change. The initial rapid rate may correlate with the merging of the irregular crack front created by the linear array of nanoindentations. In this experiment, the stress intensity was near the fracture toughness and a small crack extension was sufficient to cause failure. The rate of frequency change decreased to a lower value until the device finally failed. This result indicates an indifference to the value of stress intensity in the final stages of crack growth because the stress intensity increases as the crack grows. Some other reaction rate–limiting process may then be controlling crack growth. This result was unexpected because the static fatigue of silica on a macroscopic scale at moderate stress intensities depends exponentially on the stress intensity (*15*).

Bhaduri and Wang (6), the only other investigators to observe rate-dependent crack extension in silicon, found that the crack growth rates depended on stress intensity and were many orders of magnitude higher than those that we measured. Their experiments, however, were on much larger test specimens. Wiederhorn (*3*) also indicated that there is no apparent lower bound or fatigue limit to crack propagation in silica glass, although he concluded that better experimental design methods were necessary to investigate lower crack growth rates. The final rate of change in frequency in our experiment translates to a crack growth rate of approximately 2×10^{-11} m/s or 12 Å/min. Although this rate is very small for macroscopic devices, it can lead to relatively short failure times for materials with micrometer dimensions.

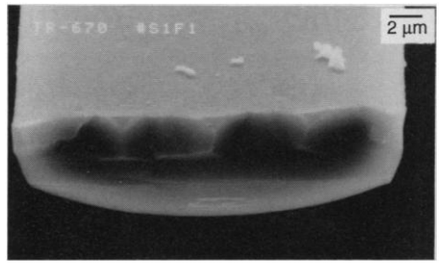

Fig. 3. Scanning electron micrograph of the fracture surface. The row of regular indentations was used to produce a continuous crack across the top of the beam.

Figure 3 is a micrograph of the fracture surface for a failed device. The crack front merges into a planar front that propagates perpendicular to the axis of the beam, that is, perpendicular to the maximum tensile principal stress. The beam then fails statically, after which the crack then changes direction and propagates along a (111) close-packed plane. We postulate that the first planar front growth of the crack corresponds to static fatigue of the silica layer on the silicon surface. The amorphous silica layer forms immediately upon exposing silicon to oxygen (*16*), so the crack growth through the silica is indifferent to the crystallographic orientation of the underlying silicon. The point of static failure where the stress intensity exceeds the inherent fracture toughnesses of silica and silicon then causes the crack to propagate along the crystallographic plane of lowest fracture toughness, that is, a (111) plane.

There is no question that the presence of water accelerates or initiates crack propagation. We have resonated a structure in a dry air atmosphere for 1 week without crack growth. Upon the addition of humidified air, crack growth was immediate and rapid. Figure 4 demonstrates the change in resonant frequency of a device, once humidified air is introduced. We believe that the above results provide an unambiguous demonstration of rate-dependent crack growth, most likely static fatigue, in room-temperature silicon.

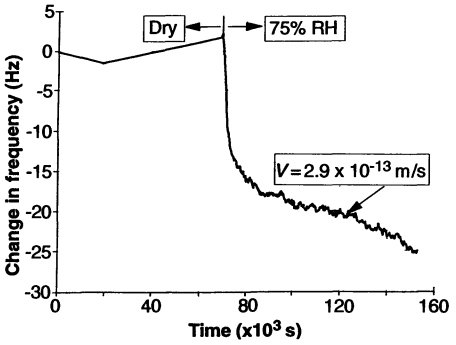

Fig. 4. Change in resonant frequency upon the addition of humid air; RH, relative humidity. The change in frequency represents immediate crack growth.

The actual mechanism governing the rate-dependent crack growth in silicon has not been well characterized. The crack growth rate does not accelerate with increasing crack length, which indicates that this rate is independent of the magnitude of the stress intensity. One possible explanation for this independence is some rate-limiting mechanism associated with either reaction rates at the crack tip or delivery of species from or to the crack tip region.

Several difficulties with the current device remain to be resolved. First, although we have good correlation between the model and device behavior, we believe that it is important to model the structure in its actual nonlinear form. Second, the stress intensity estimates assume a deep cracked beam with rectangular cross section. The actual cross section of the beam deviates from a true rectangle. Third, because we deduce crack growth from frequency shifts, we need to perform measurements of crack length based on interrupted experiments in which we measure crack length by breaking and examining fracture surfaces, using a method to mark the exposed crack, or by static compliance using a nanoindenter as a force-displacement test machine.

We have concentrated on doped, single-crystal silicon in this initial effort because in this way we eliminated the complexity associated with deposited microstructures had we used polysilicon or some other polycrystalline material. The susceptibility to rate-dependent failure should increase with polycrystalline microstructures (*17*). Moreover, dynamic fatigue will definitely be possible in materials that have greater dislocation mobilities than silicon.

REFERENCES AND NOTES

1. K. D. Wise and K. Najafi, *Science* **254**, 1335 (1991).
2. T. A. Michalske and B. C. Bunker, *J. Appl. Phys.* **56**, 2686 (1984).
3. S. M. Wiederhorn, *Fracture Mech. Ceram.* 1974, 613 (1974).
4. T.-J. Chen and W. J. Knapp, *J. Am. Ceram. Soc.* **63**, 225 (March 1980).
5. B. Wong and R. J. Holbrook, *J. Electrochem. Soc.* **134**, 2254 (1987).
6. S. B. Bhaduri and F. F. Y. Wang, *Fracture Mech. Ceram.* **1983**, 327 (1983).
7. C. P. Chen and M. H. Leipold, *NASA Tech. Brief* **10**, Item 106 (1986).
8. M. D. Thouless and R. F. Cook, *Appl. Phys. Lett.* **56**, 1962 (1990).
9. T. P. Weihs, S. Hong, J. C. Bravman, W. D. Nix, *J. Mater. Res.* **3**, 931 (1988).
10. S. Johansson, J. Schweitz, L. Tenerz, J. Tiren, *J. Appl. Phys.* **63**, 4799 (1988).
11. L. Fan, R. T. Howe, R. S. Muller, in *IEEE Micro-Electro-Mechanical Systems Workshop*, 20 to 22 February 1989, Salt Lake City (IEEE, Piscataway, NJ, 1989), p. 40.
12. S. Murakami, *Stress Intensity Factors Handbook* (Pergamon, Elmsford, NY, 1987).
13. J. A. Connally and S. B. Brown, in *Proceedings of the Sixth International Conference on Sensors and Actuators* (IEEE, Piscataway, NJ, 1991), p. 953.
14. D. Broek, *Elementary Engineering Fracture Mechanics* (Sijthoff & Hoordhoff, Alphen aan den Rijn, The Netherlands, 1978), chap. 13.
15. C. P. Chen and M. H. Leipold, *Am. Ceram. Soc. Bull.* **59**, 469 (1980).
16. S. K. Ghandhi, *VLSI Fabrication Principles* (Wiley, New York, 1983), chap. 7.
17. L. Ewart and S. Suresh, *J. Mater. Sci.* **22**, 1173 (1987).

18. We acknowledge the support of the Charles Stark Draper Laboratories and the particular assistance of B. Boxenhorn and P. Greiff. Substantial assistance was also provided by A. Taylor of AT&T Laboratories and M. Ferber of the High Temperature Materials Laboratory at Oak Ridge National Laboratory.

28 February 1992; accepted 17 April 1992

How to Make Water Run Uphill

Manoj K. Chaudhury and George M. Whitesides

A surface having a spatial gradient in its surface free energy was capable of causing drops of water placed on it to move uphill. This motion was the result of an imbalance in the forces due to surface tension acting on the liquid-solid contact line on the two opposite sides ("uphill" or "downhill") of the drop. The required gradient in surface free energy was generated on the surface of a polished silicon wafer by exposing it to the diffusing front of a vapor of decyltrichlorosilane, $Cl_3Si(CH_2)_9CH_3$. The resulting surface displayed a gradient of hydrophobicity (with the contact angle of water changing from 97° to 25°) over a distance of 1 centimeter. When the wafer was tilted from the horizontal plane by 15°, with the hydrophobic end lower than the hydrophilic, and a drop of water (1 to 2 microliters) was placed at the hydrophobic end, the drop moved toward the hydrophilic end with an average velocity of ~1 to 2 millimeters per second. In order for the drop to move, the hysteresis in contact angle on the surface had to be low (≤10°).

The motion of liquid drops on surfaces that is induced by thermal gradients has been observed experimentally and discussed theoretically (*1–4*). This type of drop motion is a consequence of the Marangoni flow within the drop that is set up by thermal gradients. Motion of liquid driven by Marangoni flow is also evident in the classical "tear of wine" effect (*5*). Evaporation of alcohol from the liquid-solid meniscus creates a local rise of the surface tension in the liquid, which induces a surface flow (and in turn a bulk flow) of wine on the wall of the wine glass; the accumulating liquids return in the form of drops. Cottington *et al.* reported that drops of several oils moved freely on a stainless steel surface when the oils contained certain types of surfactant additives (*6*). The authors postulated that the nonuniform evaporation of the surfactant resulted in a surface tension gradient in the liquid drop; this gradient caused the drops to move. This motion appears to be another example of the Marangoni effect.

M. K. Chaudhury, Dow Corning Corporation, Midland, MI 48686.
G. M. Whitesides, Department of Chemistry, Harvard University, Cambridge, MA 02138.

We report a new type of drop motion that is induced entirely by a surface chemical gradient of a solid substrate. What distinguishes the motion described here from the motions reported earlier (*1*, *2*, *4–6*) is the fact that no Marangoni forces act on the liquid—instead, the motion results from the imbalance of the surface tension forces acting on the opposite sides of the drop edge. Figure 1 represents a cross section of a water drop placed on a surface that has a spatial gradient in the surface free energy. The unbalanced Young's force (dF_Y) experienced by this section of the drop is given by Eq. 1

$$dF_Y = [(\gamma_{SV} - \gamma_{SL})_A - (\gamma_{SV} - \gamma_{SL})_B]dx \quad (1)$$

Here, γ_{SV} and γ_{SL} are the surface free energies of the solid-vapor and solid-liquid interfaces and dx is the thickness of the section of the drop. If θ_A and θ_B represent the local contact angles at points A and B, then Eq. 1 can be represented as

$$dF_Y = \gamma_{LV}(\cos\theta_A - \cos\theta_B)dx \quad (2)$$

The surface free energy of the liquid-vapor interface is γ_{LV}. The net force (F_Y) experi-